Natural Resources Canada | Ressources naturelles Canada

GEOLOGICAL SURVEY OF CANADA
OPEN FILE 8174

Near-bed hydrodynamics and sediment transport processes at the head of Logan Canyon on the central Scotian Slope

M.Z. Li, R.H. Prescott, and A.G. Robertson

2017

Celebrating 175 yrs

Canada

GEOLOGICAL SURVEY OF CANADA
OPEN FILE 8174

Near-bed hydrodynamics and sediment transport processes at the head of Logan Canyon on the central Scotian Slope

M.Z. Li[1], R.H. Prescott[2], and A.G. Robertson[1]

[1]Geological Survey of Canada (Atlantic), 1 Challenger Drive, Dartmouth, Nova Scotia

[2]Prescott and Zou Consulting, 6 Glenn Drive, Halifax, Nova Scotia

2017

doi:10.4095/299794

This publication is available for free download through GEOSCAN (http://geoscan.nrcan.gc.ca/).

Recommended citation
Li, M.Z., Prescott, R.H., and Robertson, A.G., 2017. Near-bed hydrodynamics and sediment transport processes at the head of Logan Canyon on the central Scotian Slope; Geological Survey of Canada, Open File 8174, 36 p. doi:10.4095/299794

Publications in this series have not been edited; they are released as submitted by the author.

Table of Contents

Near-bed hydrodynamics and sediment transport processes at the head of Logan Canyon on the central Scotian Slope

1. INTRODUCTION

The oil and gas industry has been shifting their exploration focus to the deep waters on the eastern Canadian margins. Pipelines that cross the slope and canyon terrain would be a likely option to transport products from the deep water to land and the market. One of the critical issues potentially affecting the exploration operations and the routing and engineering design of cross-slope pipelines is that the upper slope and canyon heads are dynamic environments with great potential of seabed mobility (King et al., 2002; Campbell and MacDonald, 2006). Transport of sediment into deep water areas down canyons is important for evaluating hazards to deep-water fibre-optic cables, monitoring the dispersal of pollutants into the deep ocean, and assessing benthic habitat in submarine canyons. We know very little of what are the physical processes and what are the magnitude and frequency of sediment mobility on the upper slope and in the canyons on the Atlantic margins.

The Geological Survey of Canada-Atlantic (GSCA) deployed the instrumented seabed lander RALPH (Heffler, 1996; Li and Heffler, 2002) in August 2005 in 278 m depth at the head of Logan Canyon (Figure 1) to obtain the first field observations of near-bed hydrodynamics and sediment transport processes on the floor of a canyon on the Scotian Slope. This report describes the seabed instrumentation and presents the preliminary results of hydrodynamics and sediment mobility observations obtained from this deep-water lander deployment. The raw and processed data obtained from this deployment will be archived at the Curation of GSCA. Following this Introduction, the lander instrumentation and deployment operation will be described in Section 2. Observation results of near-bed hydrodynamics and sediment transport processes are presented in Sections 3 and 4 respectively. Preliminary findings will be summarized in Section 5.

2. INSTRUMENTATION AND DEPLOYMENT LOCATION

2.1 Deployment and Recovery

The GSCA instrumented seabed lander RALPH was deployed at 09:20 ADST (Atlantic Daylight Saving Time) on August 12th, 2005, at the head of Logan Canyon (Figure 1) via a ship of opportunity on CCGS Sir William Alexander (Expedition 2005102). The deployment site was

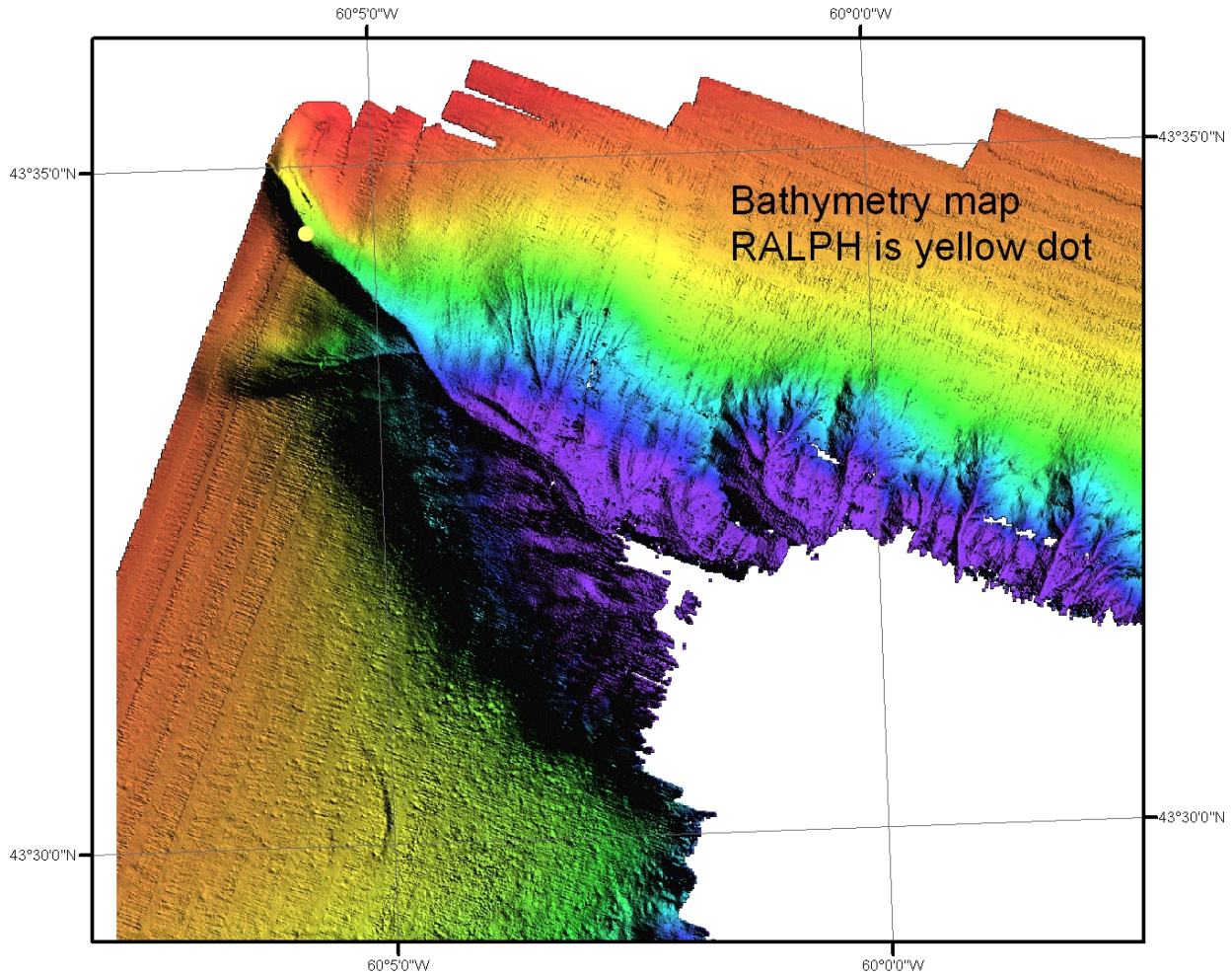

Figure 1 Map showing the location (yellow dot) of the deployed seabed lander in the thalweg at the head of Logan Canyon, on central Scotian Slope. The background shows the multibeam bathymetry with red to blue representing 100 m and 500 m depths respectively.

at 43° 34.5162′N 60° 05.6838′W, approximately in the thalweg of the canyon head in ~278 m depth. Several attempts were made to take grab samples with a medium size van Veen grab sampler. The second attempt was relatively successful and was approximately 1/8 full of fine sand with a small percentage of mud. A surface sample (0 – 2 cm) was taken for grain size analysis. A bulk sample was taken and placed in a plastic bag for sensor calibration purpose.

If the deployment of RALPH at Logan Canyon went smoothly, then the recovery of the lander was full of ups and downs but with a story book ending. Similar to the protocol of typical GSC lander deployments, the planned duration of the Logan Canyon deployment was about one month. The first recovery attempt was made on board of the DFO October 2005 Hudson expedition (thanks to collaboration of Don Gordon and John Anderson of DFO). When Hudson arrived at the deployment site on October 5th, visual search could not find the surface float that

was tethered to RALPH. With the help of GSC scientist Gordon Fader, three sidescan lines were run and the location of RALPH was confirmed. The mooring line was also fouled with the sidescan fish towing line. Hudson returned on October 6th and spent several hours dragging the area with grapples but to no avail. It was suspected that the mooring rope may have been severed at depth. With the terrain in which RALPH was deployed our best possible chance of recovery was an ROV deployment to connect a new lifting tether so that RALPH can be lifted from the sea floor. Through the connection of Dick Pickrill (the manager of Geosciences for Ocean Management Program), we contacted DND Route Survey Officer Lt. Cdr. Jim Bradford for possible help to recover RALPH using DND's fleet diving ROV. Unfortunately the scheduling of the DND's ROV meant that the earliest they could help with the recovery would be spring 2006. Options of using various commercially available ROV via Coast Guard ship of opportunity were then explored. However, factors of budget and Coast Guard ship availability did not allow these options of early recovery of RALPH. We thus returned to the original DND ROV option. Finally on 1 July, 2006, DND's fleet diving ROV DSIS (Deep Seabed Intervention System) on board CCGS Sir Wilfred Grenfell arrived at the RALPH deployment site to recover the lander. After several search dives and completing a 3 hour grid search on 2 July, RALPH was discovered at 43° 34.5043′N 60° 05.6209′W. Issues with the hydraulic motor and strong winds hampered the actual recovery operation but RALPH was successfully recovered at 11:48 on 4 July 2006 thanks to the excellent work by the DND's DSIS ROV unit and the crew of CCGS Sir Wilfred Grenfell. RALPH was returned to BIO on 7 July, 2006. The seabed lander was inspected and data were downloaded. It was found amazingly that most sensors and electronics survived after spending almost one year on the seabed in 280 m water depth and RALPH recorded nearly 2 months data.

2.2 Instrumentation

RALPH is an autonomous instrumented platform (Figure 2) for long-term near-bottom measurements of wave-current dynamics and sediment transport processes in marine environments. Detailed descriptions of the system have been given by Heffler (1996) and Li and Heffler (2002).

Table 1 summarizes the sensors on RALPH and the variables they were intended to measure for this deployment. The key sensors include: 4 Electro-Magnetic Current Meter (EMCM), 6 Optical Backscatter Sensor (OBS), 2 Acoustic Backscatter Sensor (ABS), a RDI pulse-coherent acoustic Doppler current profiler (PCADCP), and a Sony Digital Video camera (BurstCam). Five

Figure 2 Photograph of the sediment dynamics instrumented seabed lander RALPH.

sediment traps (SedTrap) were also mounted at various heights. The top plan view of the positions of these sensors on the RALPH quad frame is shown in Figure 3. The reference origin of the X and Y is the center of the vertical leg nearest to the BurstCam. Viewed from the top by standing behind the northeastern side of the quad frame (Figure 3), X positive is to the northwest and Y positive is to the southwest, and Z positive is upward from the seabed. The compass reading gave that the RALPH heading (along Y positive) was 254° magnetic north and X positive was thus to 344°, approximately along the up-canyon direction. The magnetic declination for August 2005 at the deployment location was 19° 6.36' W. The magnetic declination was not corrected in data processing and thus all directions in this report are relative to the magnetic north.

Table 1 Sensor descriptions and positions on the RALPH frame. The abbreviation of sensors and the definition of the X, Y and Z coordinates are given in the text. See Fig. 3 for the plan view of sensor positions.

Sensor	**Variable Measured**	**Position (X, Y, Z in cm)**	
Pressure Sensor	depth; wave height		138, -89, 152
Compass/Tilt	direction; tilt		134, -105, 152
RDI PCADCP (Beam 3 points to the x/y origin)	high-resolution velocity profiles		84, -117, 130
4 EMCM's	velocity profile	1	214, -142, 26
		2	147, -142, 49
		3	236, -142, 66
		4	252, -142, 97
6 OBS	suspended sediment concentration	1	166, -74, 13
		2	166, -74, 34
		3	166, -74, 52
		4	166, -74, 72
		5	166, -74, 92
		6	166, -74, 111
2 ABS	seabed elevation; high-resolution profiles of suspended sediment concentration	1	111, -29, 132
		2	109, -222, 128
DV Camera	bedform and sediment transport mode		107, -53, 133
SedTraps	grain size and thickness of sedimentation events	1	294, -9, 13
		2	294, 9, 34
		3	294, -9, 52
		4	285, 0, 92
		5	294, -9, 111

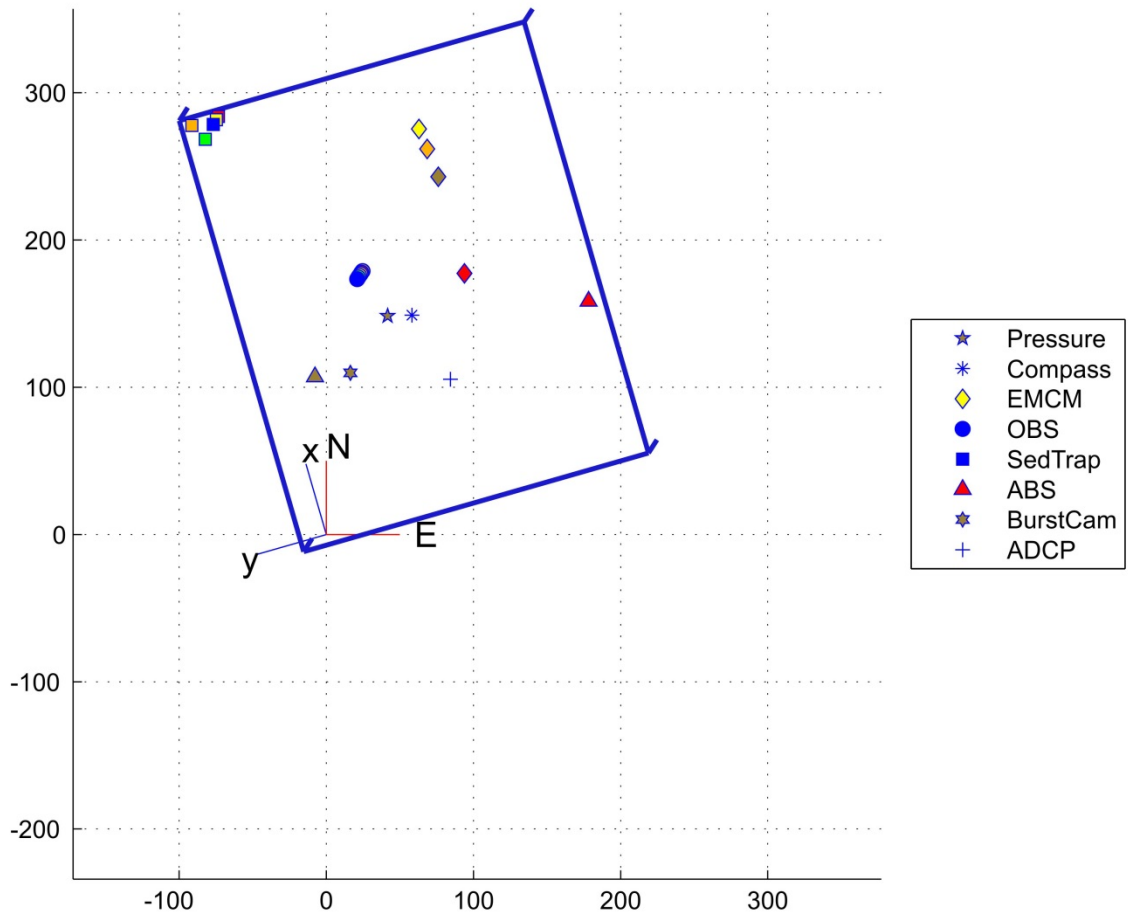

Figure 3 Top plan view of the positions of sensors on the RALPH platform. The horizontal and vertical axis show dimensions in cm. Line segments x and y represent the +x and +y directions of the lander frame coordinates. N and E respectively mark the magnetic north and east. See text and Table 1 for sensor definitions and positions.

The sampling methods and duration of useable data recorded by various sensors are summarized in Table 2. The key sensors controlled by the RALPH main computer (pressure, compass, EMCM4 and OBS6) were programmed to burst sample for 30 minutes every hour at 2 Hz. The two ABS were set up to sample at 4 Hz for a duration of 3.8 minutes each consecutively every hour. The BurstCam would record 2.1 sec takes at the beginning and end of each 30 minutes burst programmed for the key sensors logged by the RALPH main computer. The RDI ADCP was set on high resolution pulse coherent mode (Mode 8) and was programmed to burst sample for 15 seconds every 2 minutes. The sounder emitted 2 pings approximately 0.33 s apart every second and the 2 pings were averaged to produce 1 ensemble velocity profile. The

ensemble length was 1 sec and there would be 15 ensemble profiles per burst. The resolution for sampling cells was 5 cm while the vertical sampling range was from 24 cm to 154 cm below the sounder.

Table 2 Sampling methods and duration of useable data recorded by the key sensors on the RALPH frame. Sensor abbreviations are given in the text.

Sensor	Sampling method	Useable data duration
Pressure Sensor	30 minutes burst every hour at 2 Hz	~40 days (August 12 to September 21).
Compass/Tilt	Same as the pressure sensor	~64 days (August 12 to October 15)
4 EMCM's	Same as the pressure sensor	~18 days (August 12 to August 30) with poor quality
6 OBS	Same as the pressure sensor	45 days (August 12 to September 27)
RDI ADCP	15 seconds burst at 1 Hz every 2 minutes	~105 days (August 12 to November 25)
2 ABS	3.8 minutes burst at 4 Hz every hour	~52 days (August 12 to October 3)
DV Camera	2.1 sec takes every 30 minutes	~37 days (August 12 to September 18)
SedTraps	Lower traps collected accumulative sediments. SedTrap samples were stored with GSCA Curation.	

2.3 Sensor Performance and Data Quality

The pressure transducer recorded data for ~40 days (August 12 to September 21; Table 2). The pressure data drifted upward approximately linearly over the deployment duration and the linear slope was used to correct this drift. The tilt sensor (roll and pitch) and compass recorded data for ~63 days (August 12 to October 12). RALPH's pitch, roll, and compass heading are plotted in Figure 4. The pitch was -2° and stayed steady. The roll was about 2° at the start of the deployment, gradually increased to ~4° and was steady for the remaining time. The compass reading was 252° at the beginning and increased to 254° for the remainder of the deployment. These small changes in the pitch, roll and compass reading suggest that the RALPH frame was largely stable. The cause for the small gradual increase in both the roll and compass over the first few days of the deployment is unknown.

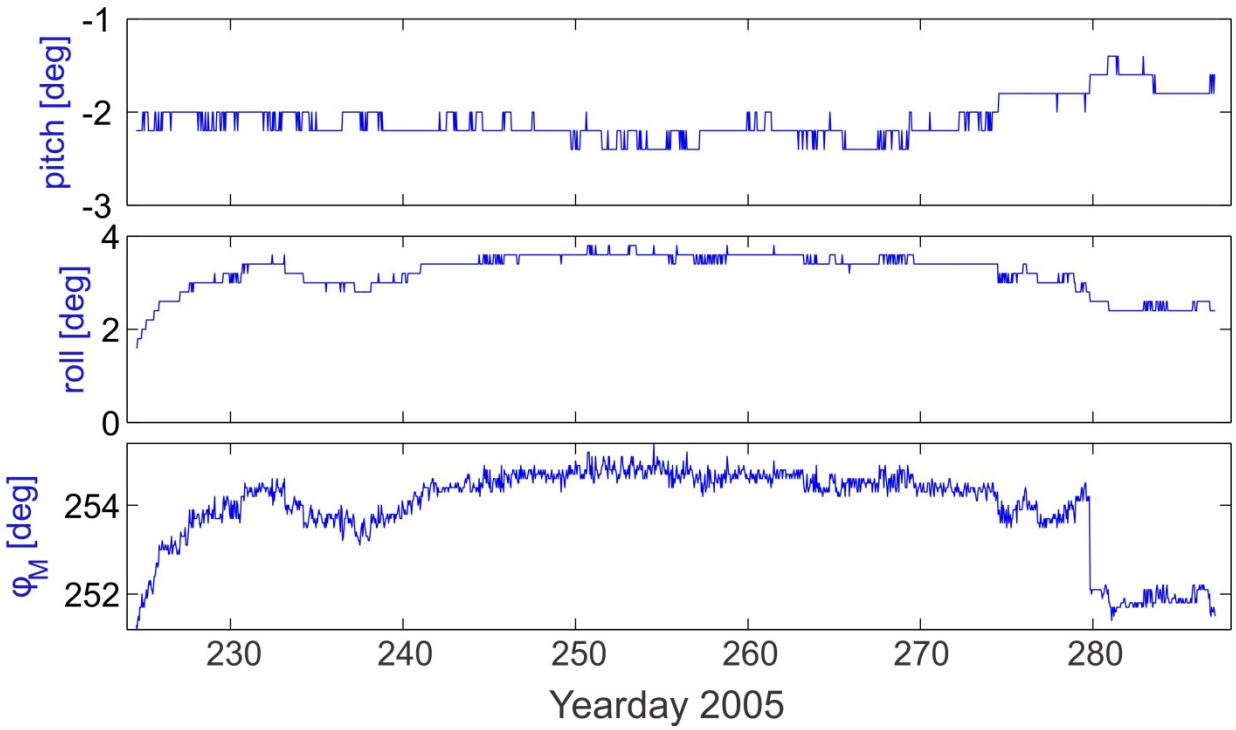

Figure 4 Time series of pitch, roll and compass reading over the deployment duration.

The EMCM4 recorded 30 min burst every hour for approximately 18 days (August 12 to 30). However, the u (easting) and v (northing) velocity components were either bad or showed vertical shifts for variable periods at different heights. Significant effort would be needed to

quality control and clean the current data recorded by the EMCM sensors. The six OBS performed well and recorded data for ~45 days (from August 12 to September 27). There is a general agreement in the variation patterns of the 6 OBS at different heights. However, the uncertainty in the calibration coefficients for zero concentration caused different offsets of OBS readings for the background suspended particulate matter concentrations so that a pattern of decreasing suspended sediment concentration with increasing heights from the sea bed could not be clearly established. The 2ABS performed well and recorded hourly burst data for ~52 days (August 12 – October 3). The RDI ADCP worked well and recorded data up to November 25 (105 days). BurstCam worked reasonably well and recorded video for about 1 hour 2 minutes which provides 4 s video of the seabed for every hour for about 37 days. The OBS and ABS sensors have not been calibrated with the in situ sediments collected in the deployment trip. Coefficients obtained from previous calibrations using similar fine sand material have been used to convert the sensor readings to engineering units of g/l or mg/l that are presented in this report.

3. NEAR-BED HYDRODYNAMIC PROCESSES

3.1 Nearbed Currents – Magnitude, Direction, and Variance

The time series of wind speed, wind direction, significant wave height and peak wave period at a grid point nearest to the 2005 Logan Canyon deployment site were extracted from the MSC50 wave model hind-cast data (Swail et al., 2006) and plotted in Figure 5 to show the environmental conditions over the lander deployment duration. The deployment period was generally under low to moderate energy conditions as wind speed was mostly less than 10-12 m/s and significant wave height was lower than 3 m. However, two moderate storms did occur respectively on year-day 255 (September 12) and year-day 261 (September 18) over which our lander recorded near-bed currents and sediment transport data. Wind speed reached 17 and 16 m/s and significant wave height reached 5.1 and 4.6 m respectively at the peaks of these storms. The effect of these storms on the bottom currents and suspended sediment concentration at the lander deployment site in the head of Logan Canyon will be explored in Section 4.3.

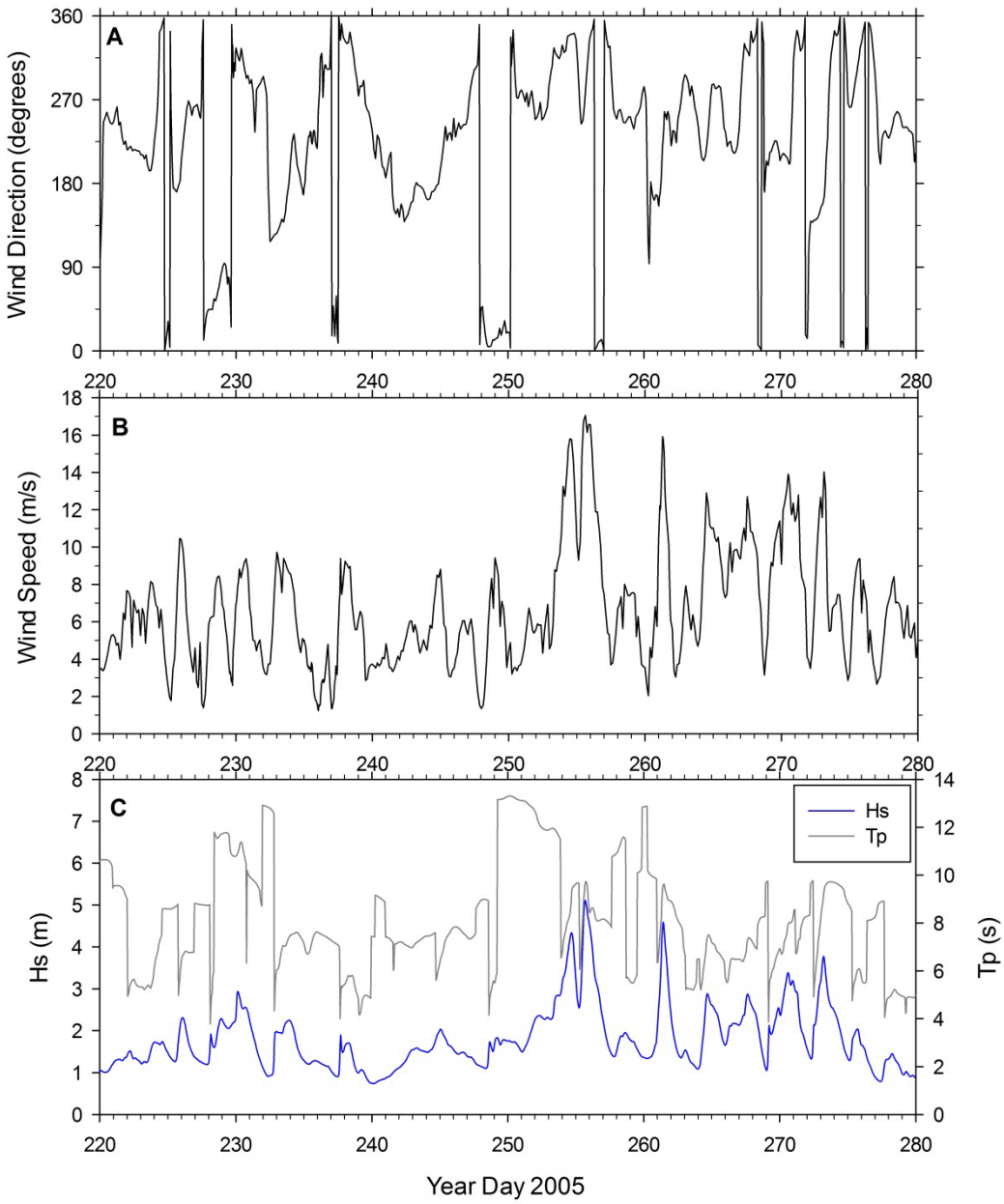

Figure 5 Time series of (a) wind direction, (b) wind speed and (c) significant wave height (H_s) and peak wave period (T_p) over the 2005 Logan Canyon deployment duration.

The time series of hourly-mean water depth, current speed at 100 cm above seabed U_{100}, and suspended sediment concentration (SSC) at about 10 cm above seabed recorded by OBS1 are plotted in Figure 6. U_{100} was obtained by averaging all the 15 seconds ADCP current data with 2 minutes interval for each hour. All the current data presented hereafter are calculated from the ADCP data unless indicated otherwise. As OBS sensors are known to be prone to data spikes, the

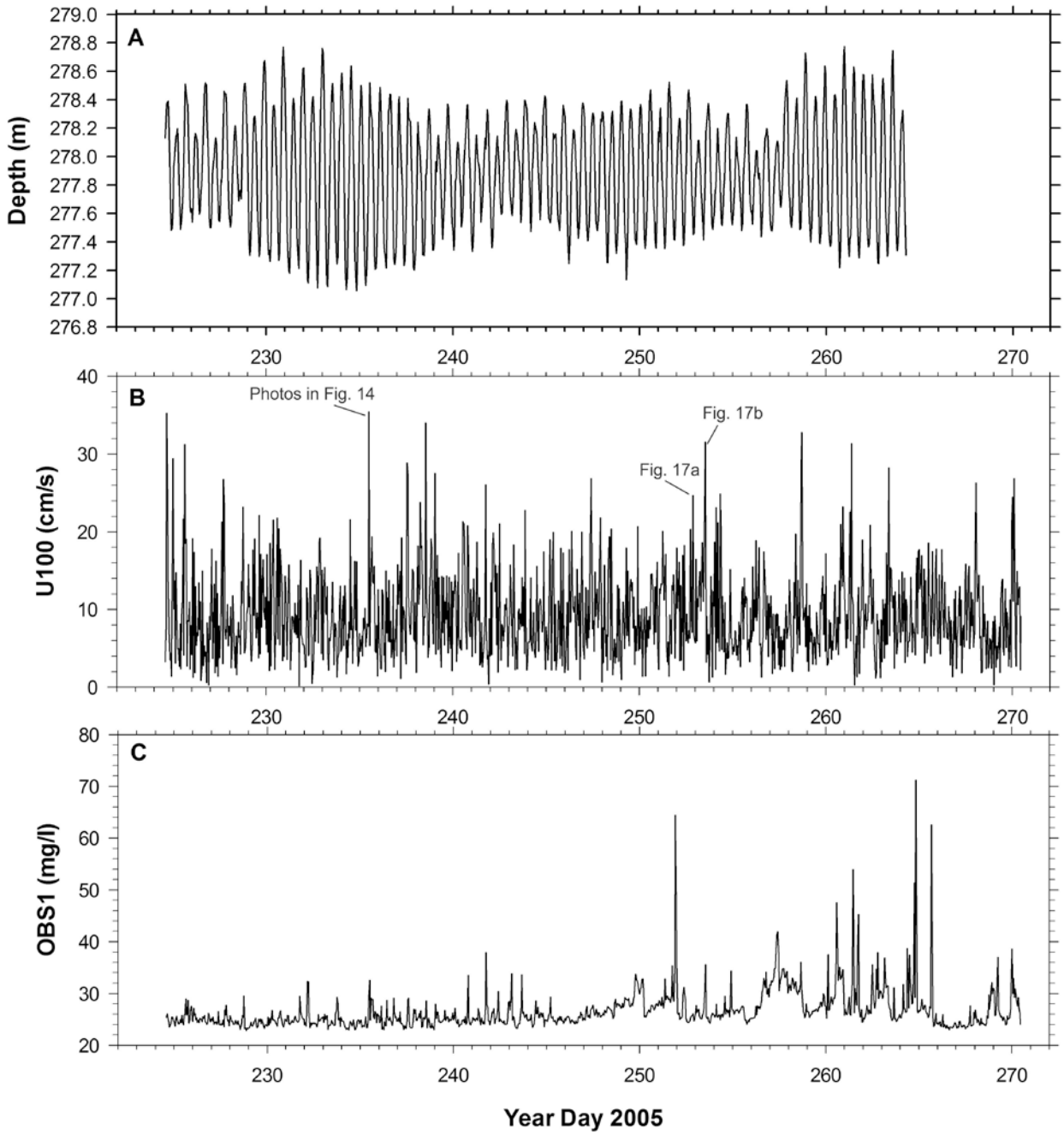

Figure 6 Time series of hour-mean (a) water depth, (b) current speed at 100 cm above seabed U100, and (c) suspended sediment concentration recorded by OBS1at about 10 cm above seabed.

OBS data in Figure 6c has been de-spiked to eliminate data that are 3 standard deviations higher than the mean value. The 2005 Logan Canyon deployment was a relatively long experiment and lasted ~46 days (~40 days for the pressure transducer). The depth data show nearly 3 spring-neap tidal cycles and the maximum tidal range was nearly 2 m (Figure 6a). The site is relatively

dynamic and the maximum mean near-bed currents often reached nearly 40 cm/s (Figure 6b). These are more than 2 times higher than the depth-mean currents predicted by tidal models (discussed in a later section). The suspended sediment concentration measured at 10 cm above seabed (Figure 6c) showed numerous resuspension events and the SSC values in these events could reach 70 mg/l but were typically 5 – 25 mg/L above the mean background value presumably due to the steady presence of fine suspended particulate matters. The SSC peaks were loosely correlated with the peaks of near-bed mean currents, and this provides further evidence for the occurrence of sediment erosion and resuspension.

Time series of the U_{100} vector and the standard deviation of the near-bed currents are plotted in Figure 7 to further demonstrate the magnitude, direction, and variance of the near-bed currents at the head of Logan Canyon. The velocity vector data in the top panel indicate that the bottom currents reached peak values of ~35 cm/s and the peak currents were predominantly in the along-canyon direction (oriented NW–SE). The strong down-canyon currents seem to occur more frequently than the up-canyon currents. Indeed the time-average of the instantaneous ADCP data gave a 4 cm/s mean current in the down-canyon direction. The stronger down-canyon currents and the down-canyon mean current imply that the mean transport should be down-canyon at the head of Logan Canyon. In such water depths, it is usually expected that tidal currents should be dominant and the variance of the bottom currents should be small. The standard deviation of the instantaneous currents (lower panel of Figure 7), however, suggests otherwise and shows that the standard deviation reached relatively high values indicating highly variable near-bed currents at the deployment site. The measured bottom currents being significantly higher than the tidal model predictions and unexpected strong variance of currents would suggest that the bottom currents at the head of Logan Canyon are strongly impacted by topographic rectification or internal tides.

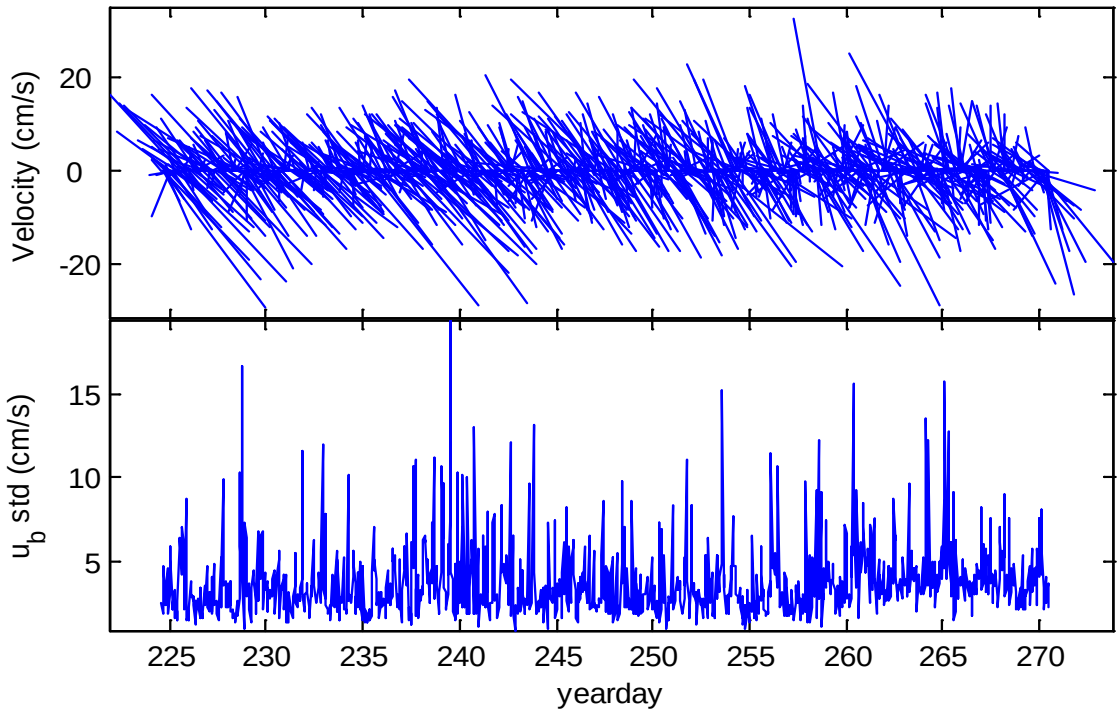

Figure 7 Time series of (top) the hourly-mean bottom current vector (magnetic north is vertical) and (bottom) the standard deviation ($u_b$std) of the instantaneous near-bed currents.

3.2 Internal Tide Processes

The time series of bottom mean currents are compared with tidal elevation for the selected period of year-day 225 to 227 in Figure 8. If the site is dominated by semi-diurnal tides, we should see two current peaks in each ebb-flood cycle. For the 2 day period, the measured bottom currents actually showed 16 peaks and some of the peaks demonstrated periods as short as 2 hours. The highly variable bottom currents thus are related to the forcing by the semi-diurnal tides but show much higher frequencies. The spectra of the along- and cross-canyon velocity components are shown in Figure 9 and the spectra were constructed by using the ADCP data for the low-frequency portion and the EMCM data for the high-frequency portion. The spectra of the along-canyon current component indeed show an energy peak at the semidiurnal tidal frequency (2 cycles per day). However, strong energy peaks are also found for currents with 4 and 6 cycles per day.

The instantaneous velocity of the u component recorded by the EMCM at 30 cm height (u30) is shown for selected bursts in Figure 10 to demonstrate the structures of the strong current peaks. The current of year-day 226 1800 (Figure 10a) represents a case of gradual change of bottom currents and current speed only decreased a few cm/s over 30 minutes. Data in the other

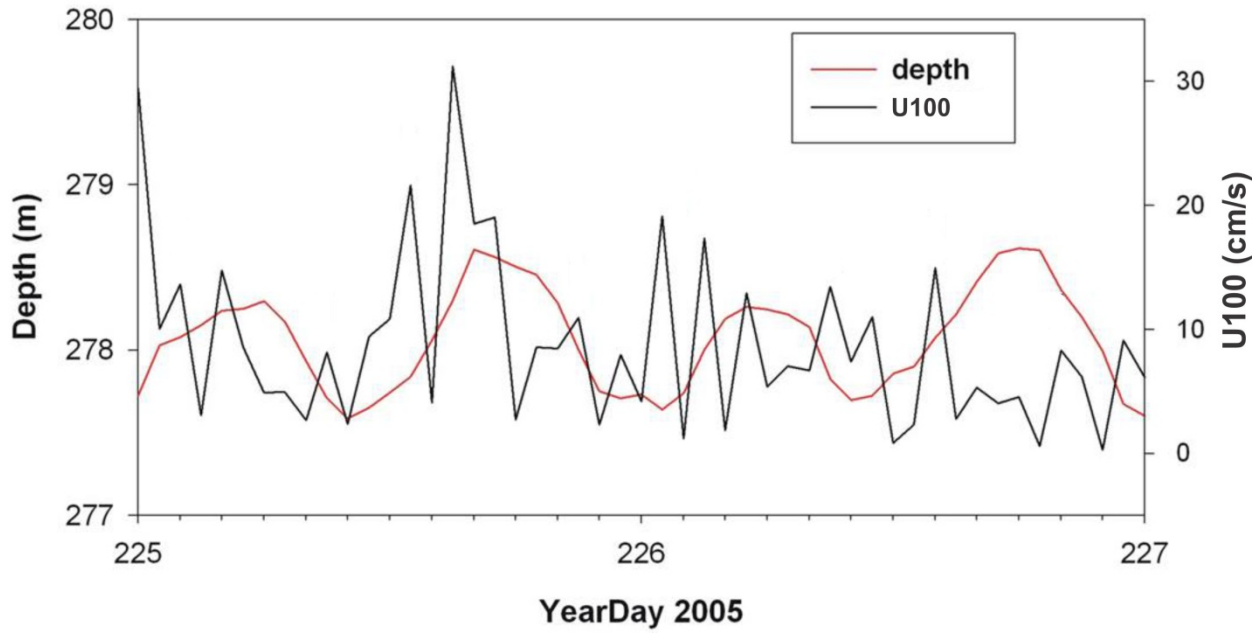

Figure 8 Time series of bottom mean currents and tidal elevation (depth) for the selected period of year-day 225 to 227 demonstrating that bottom currents are related to the semidiurnal tides but have higher frequencies.

3 panels show that the current fronts were built up quickly and the decays after the peaks were more gradual. These patterns likely represent the tidal bore features of rectified or internal tide. Particularly the data of year-day 232 2200 (Figure 10c) show that the currents changed from 10 cm/s down-canyon to ~35 cm/s up-canyon in merely 20 minutes. This swift reversal in direction and acceleration in speed would cause strong shear and turbulence that favors sediment erosion and enhances maintaining sediment particles in suspension. Besides the dominant bore features, the instantaneous current data recorded by the EMCMs also indicate the presence of internal waves with much shorter periods. For instance, the bursts of year-day 234 1800 and 227 1800 respectively show internal waves with ~80 s and 150 s periods. The individual hourly 30 minute burst data shown in Figure 10 does not present the complete view of the tidal bores and their variation over longer cycles (e.g. ebb and flood cycles). Multiple bursts of the u30 data have been mosaicked for the six hour period around year-day 232 2200 (Figure 11a) and for the two ebb-flood cycles from year-day 231-1600 to 232-1600 (Figure 11b) for a fuller understanding of the tidal bore structures and the relationship between the tidal bores and tidal elevation

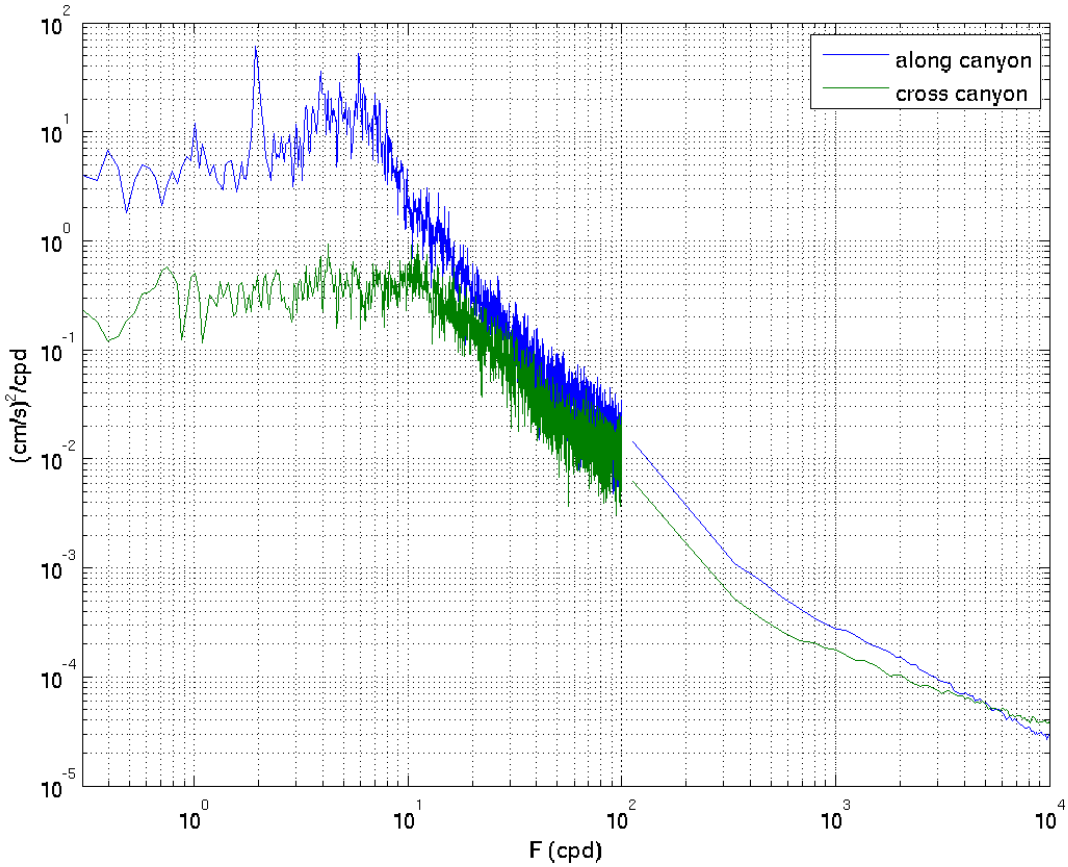

Figure 9 The spectra of the along- and cross-canyon velocity components versus frequency cycles per day (cpd) based on the bottom currents for the deployment duration. The y axis shows the spectral energy in $(cm/s)^2/cpd$ and the x axis shows the frequency F in cycles per day (cpd).

variations. It can be seen that the current peak shown by the 30 minute data of year-day 232 2200 (Figure 10c) was only part of an up-canyon tidal bore that lasted about 3 hours (Figure 11a). These measured current peaks (up to 35 – 40 cm/s) are asymmetric up- and down-canyon tidal bores which show that the up-canyon front builds up quickly and the down-canyon rush occurs more gradually. The comparison between currents and tidal elevation in Figure 11b suggests that the current bores are related to the semi-diurnal tides but have higher frequencies. Over the 24 hour period from 1600 Aug 19 to 1600 Aug 20 (Figure 11b), the depth data show two ebb-flood cycles. However, the currents show a frequency double of the tide and a ~6 hour period (i.e. 4 cycles per day). The down-canyon bores often show higher speeds (up to 35 cm/s) and last 3-5 hours while the up-canyon bores are weaker (~20 cm/s) and last only 2-3 hours (Figure 11b).

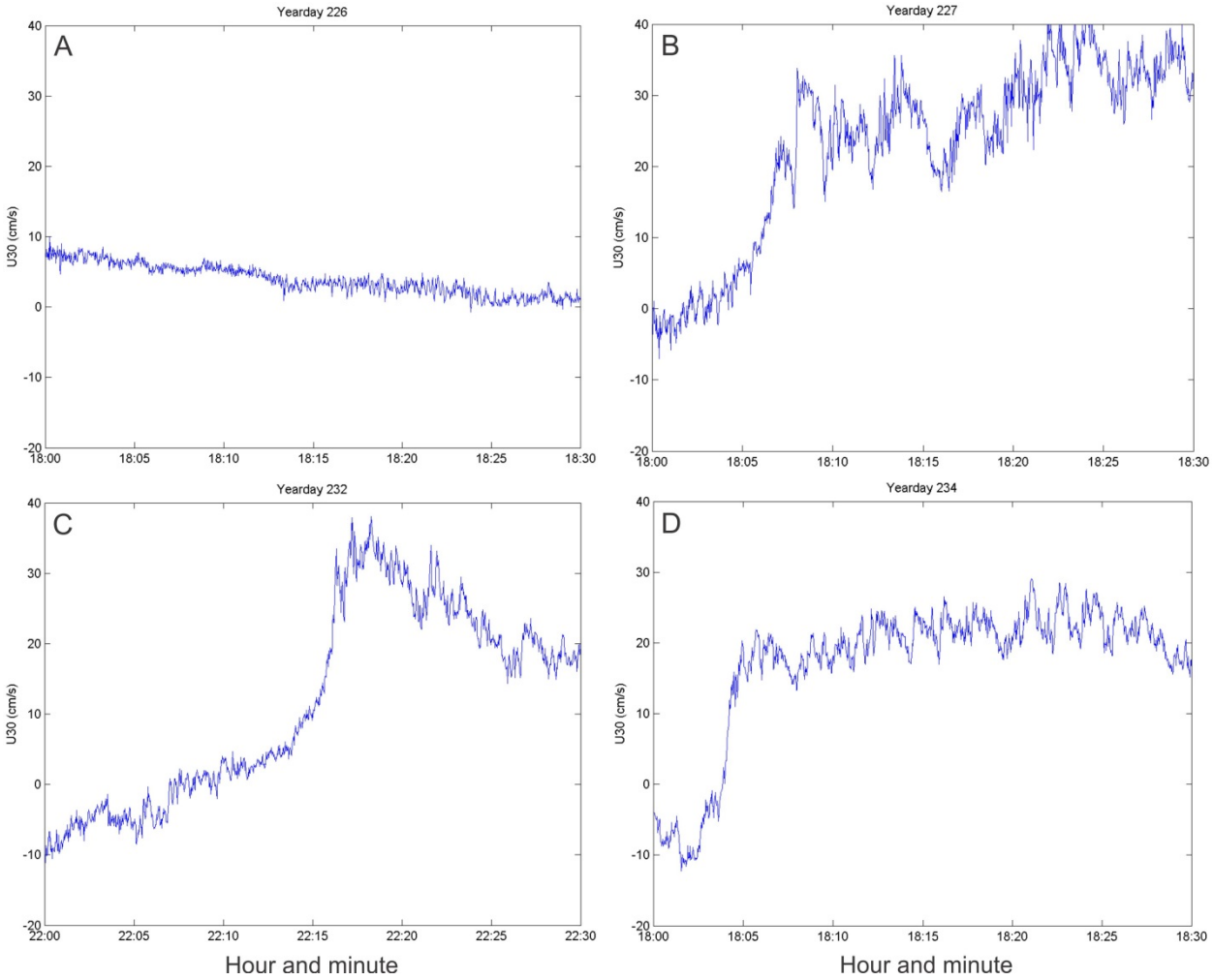

Figure 10 Time series of the instantaneous velocity of the u component measured at 30 cm above seabed (u30) for selected bursts. Year-days are labeled and hour and minutes are given by the x-axis. U30 positive is up-canyon and negative is down-canyon.

Speeds in the up-canyon bores, however, occasionally can also reach 35 cm/s (e.g. those at year-day 232 2200 shown in Figure 10c and at 1800 on August 20 shown in Figure 11b).

To further establish that the observed tidal bores were related to internal tide, the along-canyon tidal excursion distance is compared with the temperature variation for the selected period from year-day 236 to 243 (Figure 12). The along-canyon component of the hourly ADCP bottom current data were used to compute the excursion distance for each hour and the calculation was simplified by ignoring the flow expansion or contraction due to the funnel-shape of the canyon head. To facilitate the comparison, the reversed normalized temperature, which was calculated as the hourly temperature subtracting the mean temperature then normalized by

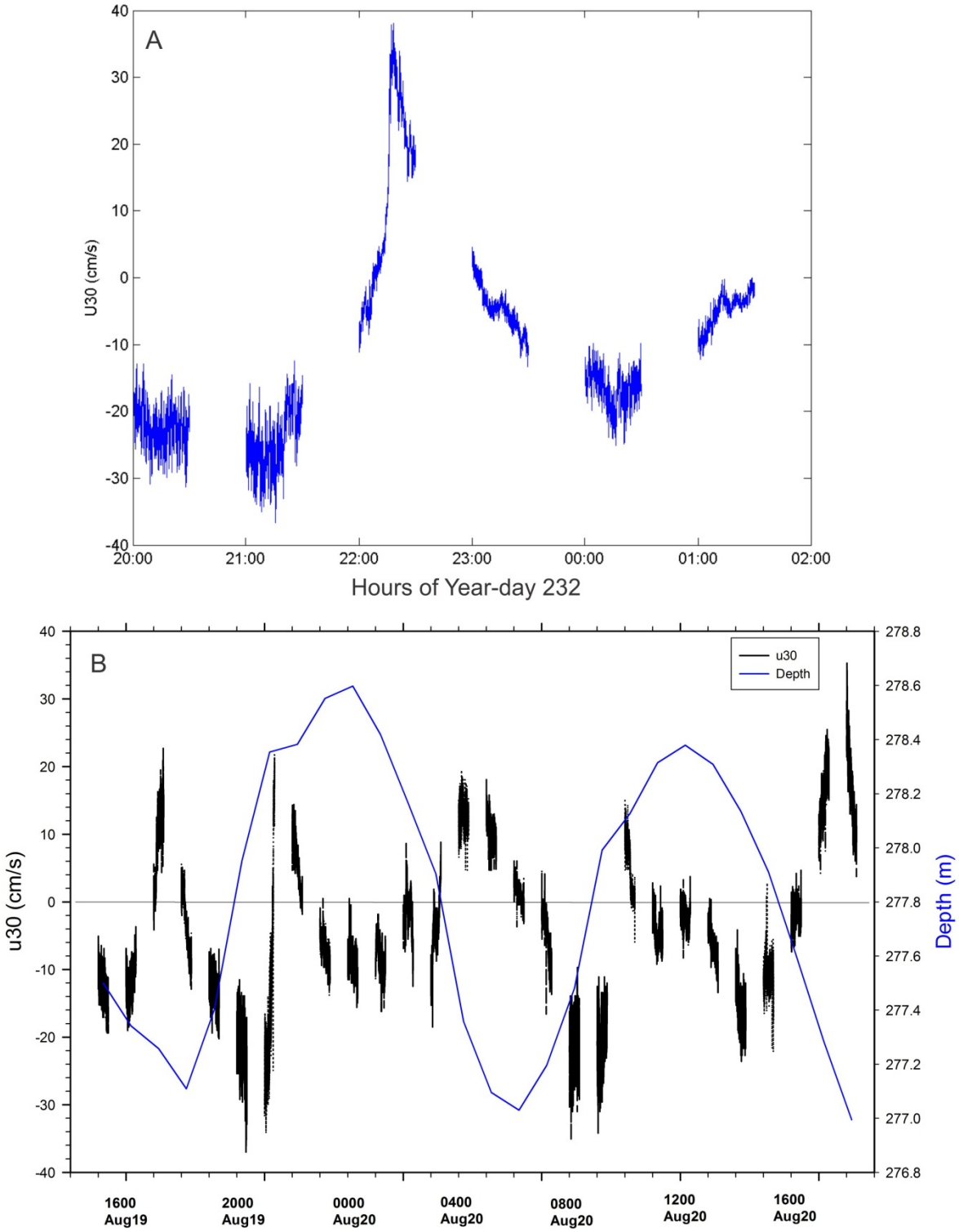

Figure 11 Mosaicked solitary bores of u-component velocity u30 for the periods (a) Year-day 232 2000 to year-day 233 0200 (2000 Aug 20 – 0200 Aug 21) and (b) year-day 231 1600 – year-day 232 1600 (1600 Aug 19 – 1600 Aug 20). Blue line in (b) is the tidal elevation.

the standard deviation, was used in Figure 12. The up- and down-canyon excursions could reach 1-2 km in Logan Canyon. The isotherms (temperature contours) were lowered (temperature decreased) when the flow was up-canyon and vice versa the water temperature increased when the flow reversed to flow down-canyon. Therefore the up- and down-canyon flows are well correlated with the fall and rise of temperature. This provides the evidence that the observed current peaks (shown in Figures 10 and 11) indeed own their genesis to internal tides. Similar internal tidal bores with periods shorter than the semi-diurnal tides have also been observed at the head of Lydonia Canyon on the southern flank of Georges Bank (Butman, 1988), at the head of the Baltimore Canyon on the US east coast (Gardner, 1989), at the head of the Monterey Canyon off central California (Rosenfeld et al., 2002) as well as on the shelf break, off Santa Monica Bay, California (Noble and Xu, 2003).

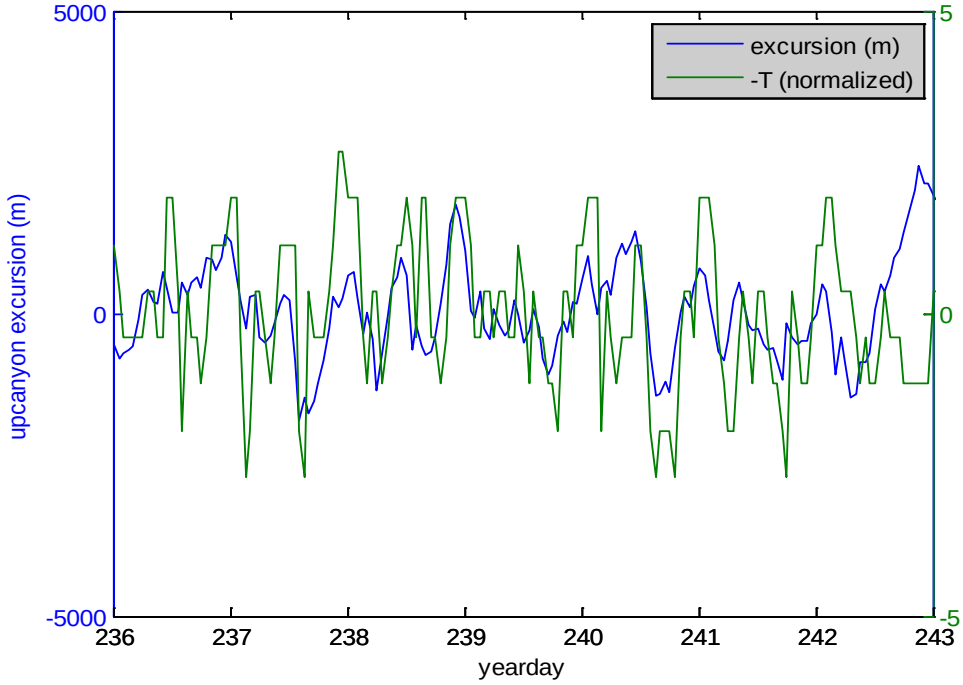

Figure 12 Along-canyon tidal excursion (in blue) compared with the temperature variation (in green) for the selected period year-day 236 to 243. Positive excursion is up-canyon. The temperature variation is shown as the reversed normalized temperature (see text for explanation).

3.3 Comparison between Lander Measurements and Tidal Model Predictions

Webtide is a widely used 2-dimensional tidal model system for tidal current predictions on the Canadian Atlantic shelf (e.g. Dupont et al. 2005; Li et al., 2015). The near-bed currents measured by RALPH at the head of Logan Canyon are compared with the depth-mean tidal currents predicted from Webtide (Figure 13) to evaluate the differences and possible implications if the model predicted currents are used in sediment transport calculations.

Webtide predicts roughly equal up- and down-canyon currents that reach a maximum of ~15 cm/s (Figure 13a, b). The RALPH data show much higher measured bottom currents. The maximum measured near-bed up-canyon velocity was ~25 cm/s and the maximum measured down-canyon velocity reached ~35 cm/s. Webtide predicts that the along- and cross-canyon currents are nearly equal in magnitude and hence a more ellipsoidal flow pattern. In contrast, the measured bottom currents are more rectilinear and along-canyon current speeds are typically 2-3 times higher than the cross-canyon flows. Furthermore, the zoomed comparison for year-day 238 to 239 (Figure 13c) demonstrates that while the Webtide predicted currents have semi-diurnal frequency e.g. two up-canyon and two down-canyon peaks per day, the lander data actually show 4 up-canyon and 4 down-canyon peaks for each day due to the effect of the internal tides. These comparisons suggest that Webtide model by design is not capable to simulate these high-frequency processes as the model does not incorporate effects of density stratification (internal tides) and the focusing of tidal energy by the high-resolution local topography in a canyon. If the tidal currents predicted by Webtide were directly used in computing sediment transport, the magnitude and frequency of sediment transport will be under-estimated. Neither will the net down-canyon transport be predicted.

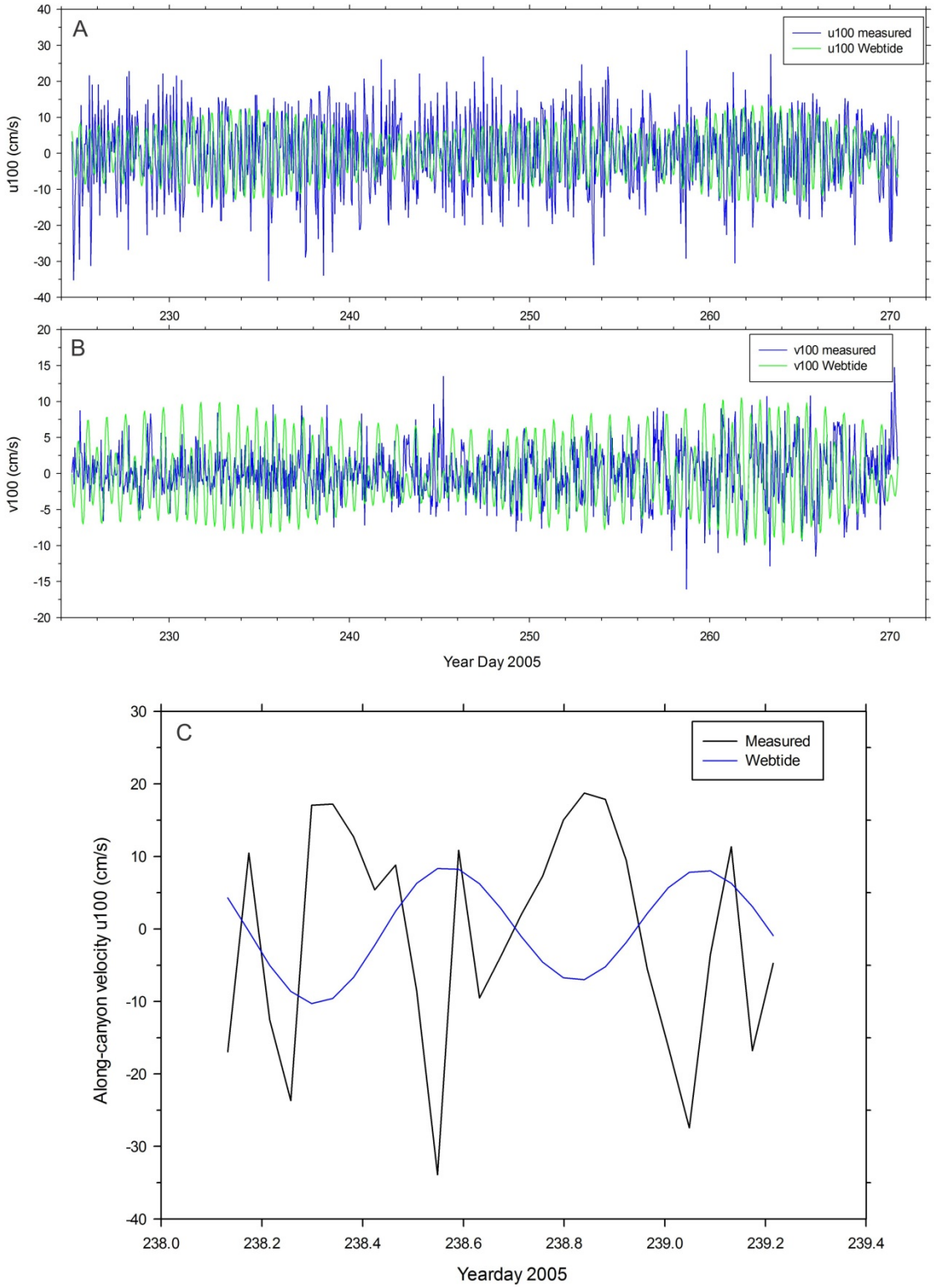

Figure 13 Comparison of measured and Webtide predicted currents at the head of Logan Canyon. (a) the along-canyon current (u100) and (b) the cross-canyon current (v100) for the deployment duration; (c) the along-canyon currents for year-day 238 to 239. Positive currents are respectively up-canyon (a, c) and to the southwest (b).

4. OBSERVATIONS OF SEABED RESPONSES AND SEDIMENT TRANSPORT

4.1 Mean Grain Size and Thresholds for Bedload and Suspended-Load Transport

A surface sample (0 – 2 cm) taken from the grab sample collected during deployment was submitted to the GSCA Sedimentology Laboratory (SedLab) for grain size analysis which showed that the bottom sediment at the deployment site is composed of fine sand with a mean grain size D = 0.19 mm. The seabed photos confirm the fine sand nature of the bottom sediments (Figure 14). Based on this mean grain size, the Yalin method according to Miller et al. (1977) was used to estimate that the critical shear velocity (shear stress in velocity unit) for bedload transport u_{*cr} is 1.27 cm/s. The critical shear velocity for suspended-load transport is defined as $u_{*crs} = 0.8W_s$ by Bagnold (1966) where W_s is the grain settling velocity. The estimated u_{*crs} is 1.49 cm/s. The drag coefficient at 1 m above bottom C_{100} is assumed to be 0.003 for unrippled sandy sediments (Dyer, 1986). With this C_{100} value and the estimated values of u_{*cr} and u_{*crs}, the quadratic stress law,

$$\tau = \rho u_*^2 = \rho C_{100} U_{100}^2 \qquad (1)$$

where τ is the bed shear stress and ρ is water density, was used to estimate that the critical current for the initiation of bedload transport, U_{100cr}, would be 23 cm/s while that for the onset of suspended-load transport, U_{100crs}, is 27 cm/s.

4.2 Observation of Bedload and Suspended-Load Transport

The purpose of the BurstCam is to monitor the morphology of possible bedforms as well sediment transport mode. The seabed images recorded by the BurstCam respectively for 1100 and 1200 on August 23 (year-day 235) are shown in Figure 14. At 1100, the bottom current was only 8 cm/s and the seabed photo shows bioturbation features and benthos tracks with no sign of sediment movement (top panel). One hour later (lower panel), U_{100} suddenly increased to 35 cm/s (Fig. 15) which exceeded the thresholds for both bedload and suspended-load transport. The seabed photo indeed shows active bedload transport and the development of asymmetric current ripples that migrate down canyon. The slight blurriness of the second photo also suggests that saltation or weak resuspension probably occurred. Active current ripples and image blurriness were observed at numerous other occasions throughout the 1 hour video recording.

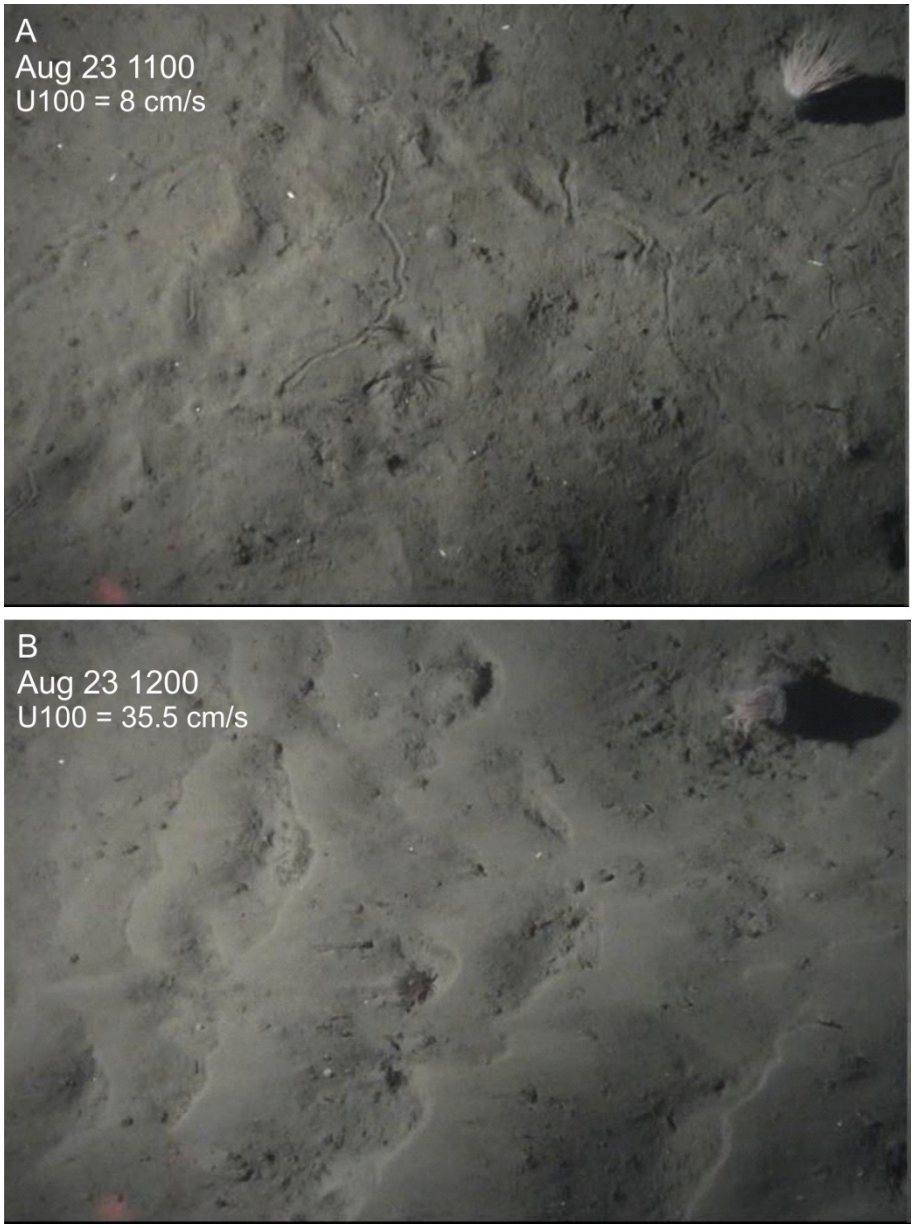

Figure 14 Seabed images recorded by the BurstCam respectively at (a) 1100 and (b) 1200 on August 23, 2005 (year-day 235). Photo top points 254° magnetic north.

Both the ABS sensors and the 6-OBS array measured the vertical profiles of suspended sediment concentration. The details of SSC variations recorded by these sensors and their correlation with the concurrently measured bottom current data are examined for selected time periods to provide evidence of sediment transport and to assess the adequacy of the estimated critical currents for bedload and suspended-load transport. Time series of the suspended

sediment concentration recorded by OBS1 (~10 cm above bottom) and OBS2 (~30 cm above bottom) are compared to the bottom current U_{100} for the period year-day 235 to 238 in Figure 15. There is a general correlation between the bottom current and measured sediment concentration and the values of SSC peaks were 5 – 10 mg/l higher than the background values. These are evidence that sediment suspension truly occurred. ABS data further corroborate the observation of sediment suspension. The profiles of instantaneous SSC recorded by ABS2 sensor for year-day 235 1200 and 253 1300 are presented in Figure 16. At year-day 235 1200 (August 23 1200), the same hour as the seabed photo shown in Figure 14a, U_{100} was 35.5 cm/s which was significantly higher than U_{100crs} = 27 cm/s. ABS recorded the strongest sediment resuspension at this hour over the deployment duration. The SSC immediately above seabed reached as high as 100 mg/l and decreased to a few mg/l at ~0.5 m above the bottom (Figure 16a). U_{100} for year-day 253 1300 was 31.6 cm/s and moderately above the value of U_{100crs}. Sediment suspension was again observed (Figure 16b) but substantially less than year-day 235 1200.

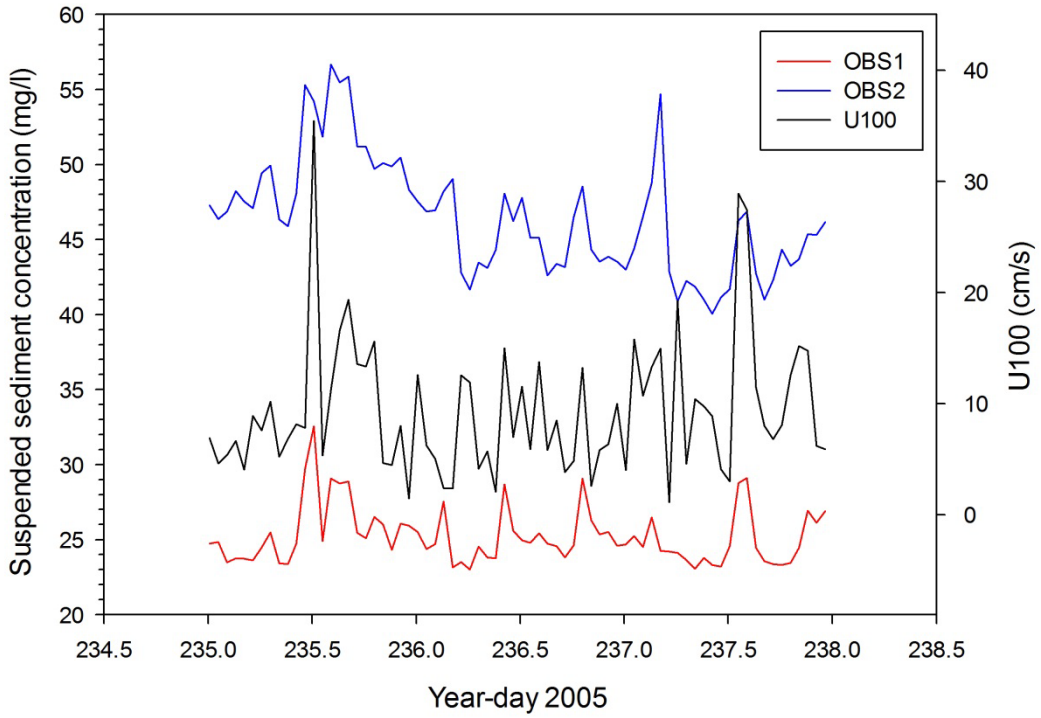

Figure 15 Time series of bottom current U100 and suspended sediment concentration recorded by OBS1 (~10 cm above bottom) and OBS2 (~30 cm above bottom) for the period year-day 235 to 238.

Near-bed currents and suspended sediment concentration measured at different heights have been examined for specific events to evaluate the adequacy of the estimated critical currents for the initiation of bedload and suspended-load transport. For the event of year-day 252 2100 (Figure 17a), U_{100} reached 24.7 cm/s which was higher than the threshold for bedload transport U_{100cr} but less than the threshold for suspended-load transport U_{100crs}. Data from OBS1 which was the closest to the seabed at10 cm height, showed slight increase of 1 – 2 mg/l above the background mean value likely due to local sediment saltation. Sediment concentration of OBS3 at ~50 cm and OBS4 at ~70 cm above the seabed, however, did not show any increase above their respective background values. The vertical patterns of suspended sediment concentration changes suggest that since bottom current only exceeded U_{100cr} and was less than U_{100crs}, only bedload transport, shown by the slight increase of sediment concentration recorded by OBS1, occurred and that sediment resuspension did not occur as OBS3 and OBS4 did not record any increase of sediment concentration. During the event of year-day 253 1300 for which the ABS data have been presented in Figure 16b, U_{100} reached 31.6 cm/s and was moderately above the value of U_{100crs}. Suspended sediment concentration recorded by all three OBS indeed showed increases above the background values (Figure 17b), indicating a resuspension event. Also the increase of SSC above the background value was the highest for the lowest OBS1 at ~10 mg/l. The increase of SSC decreased respectively to ~6 and 4 mg/l for OBS3 at ~50 cm height and OBS4 at ~70 cm height. The vertical variation of SSC observed with the OBS at various heights and the decrease of instantaneous SSC with height above seabed recorded by the ABS (Figure 16) suggest that the sediment suspension was bottom intensified. Thus the detailed analyses of the bottom currents and suspended sediment concentration data for these two events demonstrate that the estimates of the critical currents for the initiation of bedload and suspended-load transport are adequate and that the sediment suspension associated with the strong current events was from the erosion and resuspension of the local sediments.

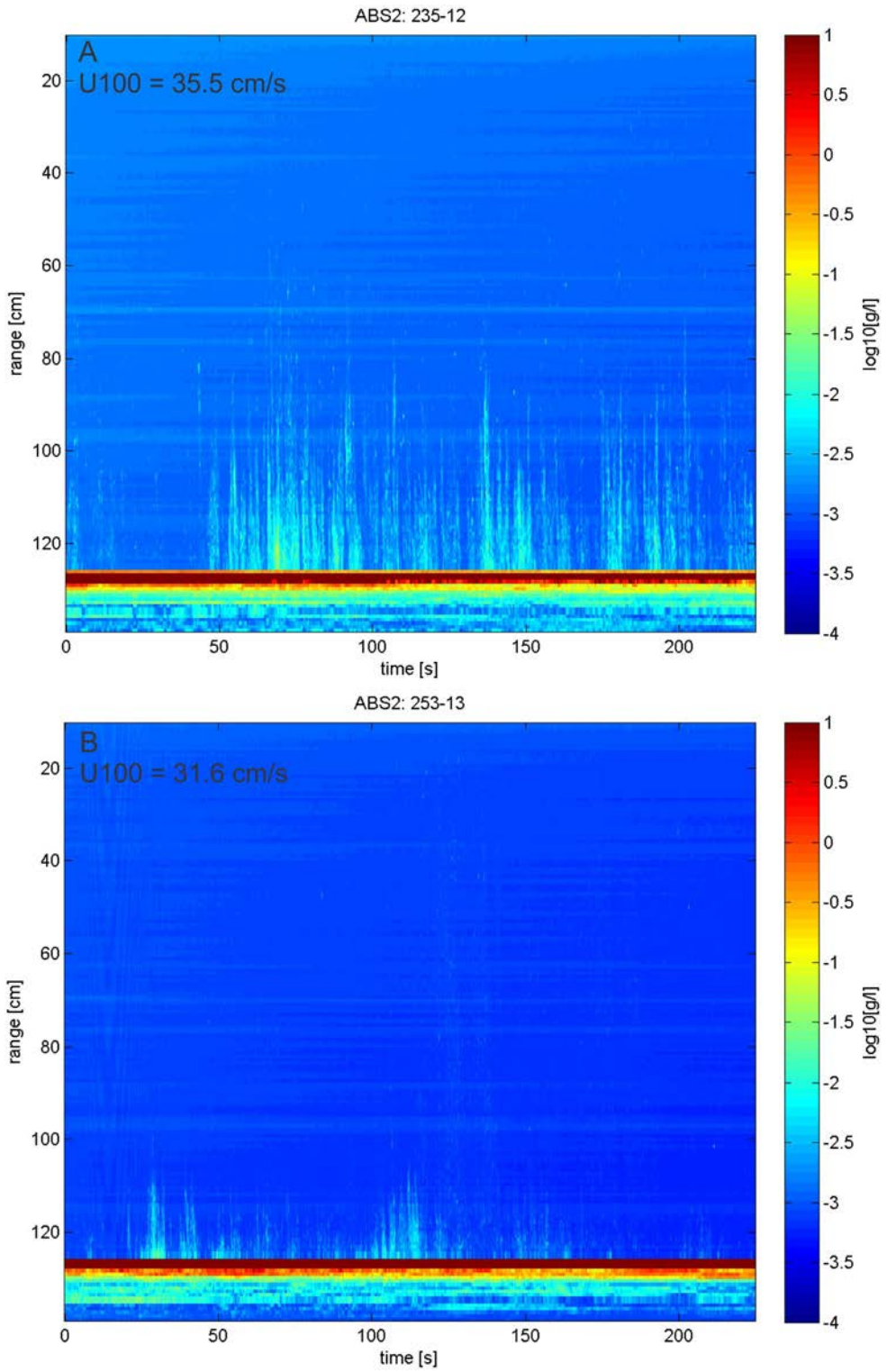

Figure 16 Suspended sediment concentration profiles recorded by ABS2 for (a) year-day 235 1200 and (b) year-day 253 1300.

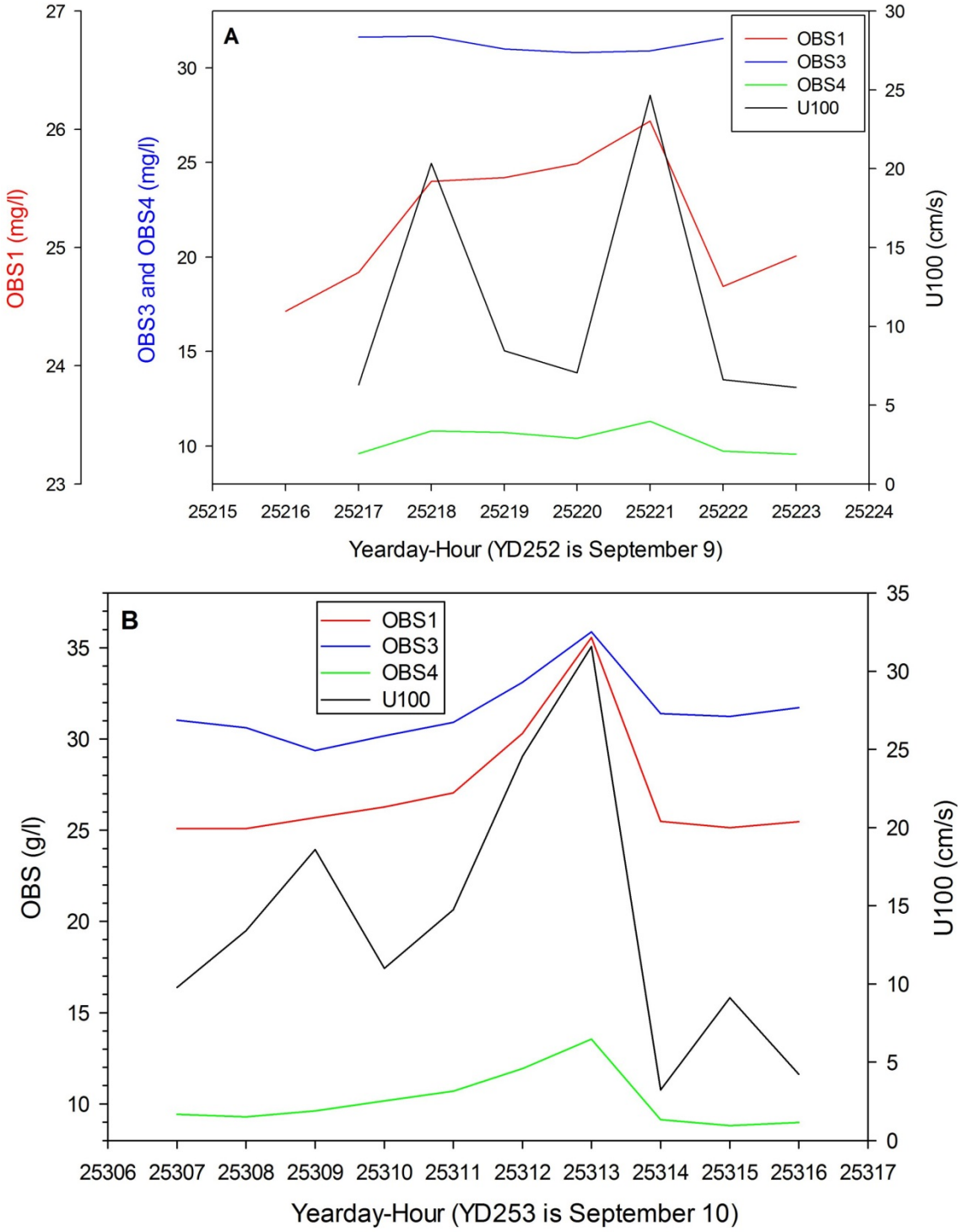

Figure 17 Near-bed currents and suspended sediment concentration for the events on (a) year-day 252 and (b) year-day 253.

4.3 Potential Effects by Storms

The wind and wave conditions over the 2005 Logan Canyon lander deployment duration (Fig. 5) indicate the occurrence of moderate storms on year-day 255 and year-day 261 respectively. The bottom currents and suspended sediment concentration measured by the lander are analyzed to assess what are the potential effects of storms on the near-bed currents and suspended sediment transport in the head of Logan Canyon. Since the effects by the two storms were found similar, the analysis is focused on the storm on year-day 255.

Strong currents up to 35 cm/s occurred at YD235.5. The measured velocity at 1 m above the bottom as well as suspended sediment concentration measured at 13 and 34 cm above bottom for this current event have been presented in Figure 15. Fig. 5 shows that the winds and waves were relatively quiescent around YD 235. Therefore the variation of SSC shown in Fig. 15 represents the response of suspended sediments to the strong current at YD235.5 with no influence of storms. As the peak currents of 35 cm/s well exceeded the threshold current for suspended-load transport U_{100crs} = 27 cm/s, both OBS sensors recorded 8-10 mg/l SSC increase above the background value. As the peak of the bottom current passed, SSC values quickly decreased to the background values in a few hours and remained low until the next strong current event just after YD237.5 (Fig. 15). Examination of SSC data during other strong current events without the influence of storms before YD255 confirmed similar SSC variation patterns.

The temporal variations of the hindcast wind speed, measured bottom current speed (U100) and suspended sediment concentration at the lowest four OBS sensor heights (13, 34, 52 and 72 cm respectively) during the storm on YD255 are shown in Figure 18. The winds and waves of the YD255 storm reached peak conditions at ~1200. The bottom currents were up to 15 cm/s and did not increase significantly at the peak of the storm and for the next 2 days after the storm. The OBS data did not show substantial increases above the background concentrations at the peak of the storm or 24 hours after the storm peak. From ~YD256.5, suspended sediment concentration gradually increased above the background values and reached peak values around YD257.4 for OBS1 and around YD258 for the other 3 OBS sensors despite that the bottom currents stayed less than 20 cm/s (Fig. 18). The greatest increase of SSC above the background level, ~60 mg/l, was measured by OBS 3 at 52 cm above bottom (cmab). The increase of SSC decreased to moderate (~30 mg/l) at 34 cmab and was further reduced to 15 mg/l for the lowest OBS at 13 cmab. Further up in the water column, OBS4 at 72 cmab only recorded an increase of 5 mg/l

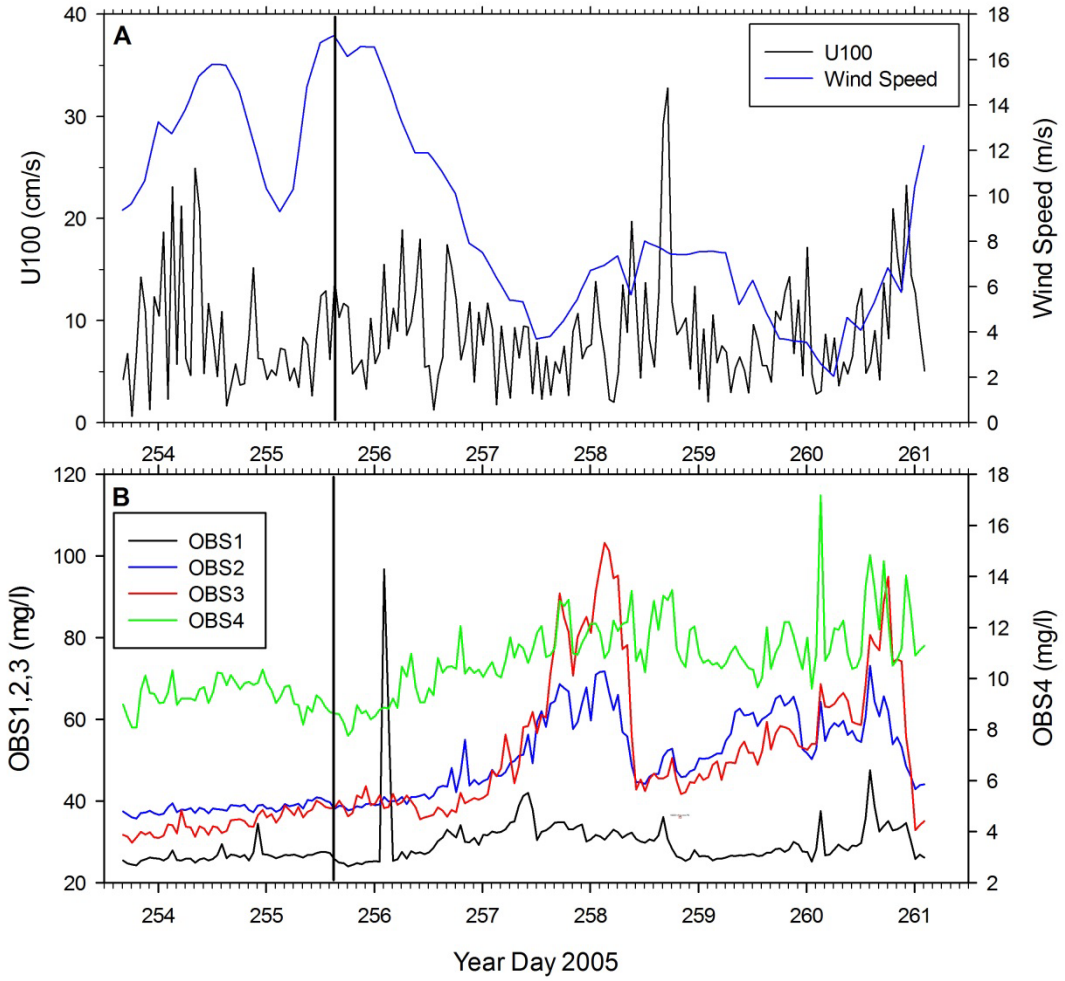

Figure 18 Time series of (a) model wind speed and measured bottom current (U100) and (b) suspended sediment concentration recorded by OBS at the lowest four heights (13, 34, 52 and 72 cm above bottom respectively) over the storm on year-day 255 marked by the thick vertical line.

from the background values. This pattern of vertical variation of SSC would suggest that this event of increased suspended sediment concentration was not bottom intensified but rather likely was adected to the lander site from the upstream part of the canyon. From YD258 to YD261, wind speed was less than 10 m/s and bottom currents were less than 20 cm/s except for a high value of 33 cm/s at YD258.7. The measured SSC values first decreased quickly to magnitudes just slightly above the background levels and then gradually increased again to reach peak values similar to those around YD258. The strong currents at YD258.7 caused small and brief increase

of suspended sediment concentration. However it could not account for the much greater increase of SSC over the two day period from YD259 to 261.

We hypothesize that these observed SSC peaks that were substantially higher than the background values and lasted more than 24 hours were likely due to the interception by the up-stream portion of the Logan Canyon of the sediment transport on the shelf and upper slope driven by the storm on YD255 (Hill and Bowen, 1983; Mosher et al., 2004). The spilled sediments were then advected down canyon to the 2005 lander site which would explain the two day lags between the peak of the storm and the peak of observed suspended sediment concentration at the lander site. The verification of this hypothesis will require concurrent lander observation at multiple locations both along the canyon and on the adjacent slope as well as detailed analysis of the magnitude and water depth of sediment transport on the shelf and upper slope during major storms.

4.4 Magnitude, Frequency and Direction of Sediment Transport

Bottom current speed U_{100} is compared against the critical velocity for bedload transport U_{100cr} and that for suspended-load transport U_{100crs} (Figure 19) to estimate the frequency of sediment transport due to the measured near-bed currents. Under the summer conditions of this deployment, fine sand sediments in the head of Logan Canyon were found to be transported in bedload in 2.1% of the time (or 18 hours/month) while suspended-load transport was less frequent and occurred in 1.2% of the time (or 9 hours/month).

Based on the measured bottom currents and observed mean grain size, the bedload transport rate Q_b has been estimated from the Einstein-Brown (Brown, 1950) bedload equation:

$$Q_b = 40WsD(\rho/\triangle\rho gD)^3 u_*^5 |u_*| \qquad (2)$$

where $\triangle\rho$ is the effective density defined as grain density ρ_s minus water density ρ, g is acceleration due to gravity, and shear velocity u_* is calculated from U_{100} using Equation (1). Suspended-load transport rate, Q_s, has been approximately estimated for the near-bed 1 m layer by multiplying U_{100} and the suspended sediment concentration measured by OBS3 at ~50 cm above bottom. Both Q_b and Q_s have only been calculated for hours when the critical velocities U_{100cr} and U_{100crs} were respectively exceeded.

The estimated bedload and suspended-load transport rates are presented in Figure 20. Maximum bedload transport reached 0.003 g/cm/s during the deployment. Bedload transport was predominantly down-canyon as peaks of down-canyon transport were stronger and occurred more frequently than peaks of up-canyon transport (Figure 20a). The residual (or mean) bedload averaged over the deployment was 1.42 x 10^{-5} g/cm/s to 159° (down canyon). The magnitudes of maximum suspended-load transport were nearly equal for up-canyon and down-canyon directions (Figure 20b). However, down-canyon transport occurred far more frequently than up-canyon transport. Therefore the suspended-load transport was also dominated by the down-canyon movements and the residual suspended-load transport was 7.4 x 10^{-4} g/cm/s to 153°. The maximum suspended-load transport rates were up to 0.15 g/cm/s which were 2 orders of magnitude greater than the maximum bedload transport. Thus suspended-load transport was dominant over bedload transport at the head of Logan Canyon.

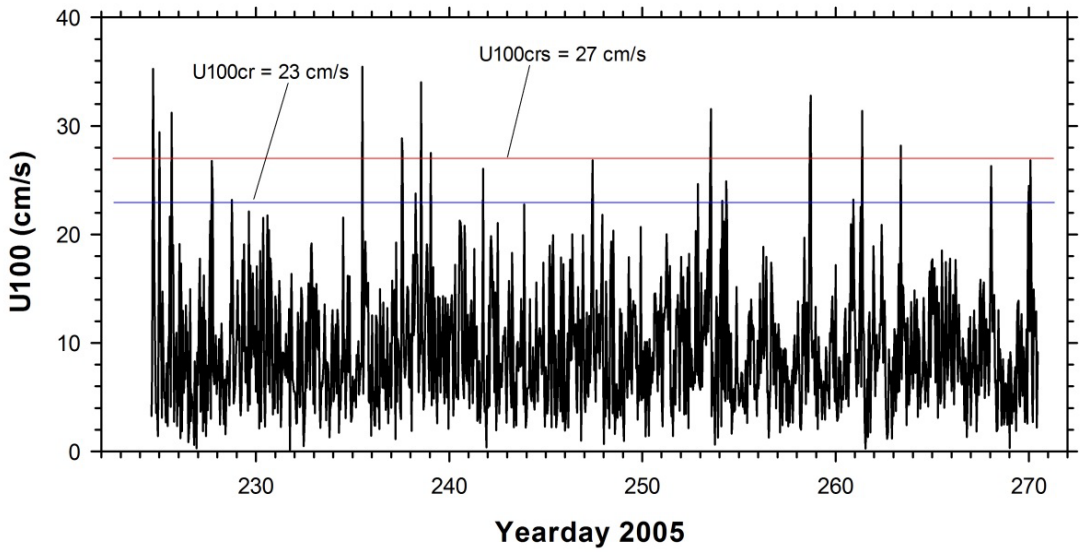

Figure 19 Bottom current speed U100 compared against the critical velocity for bedload transport U100cr (blue line) and suspended-load transport U100crs (red line).

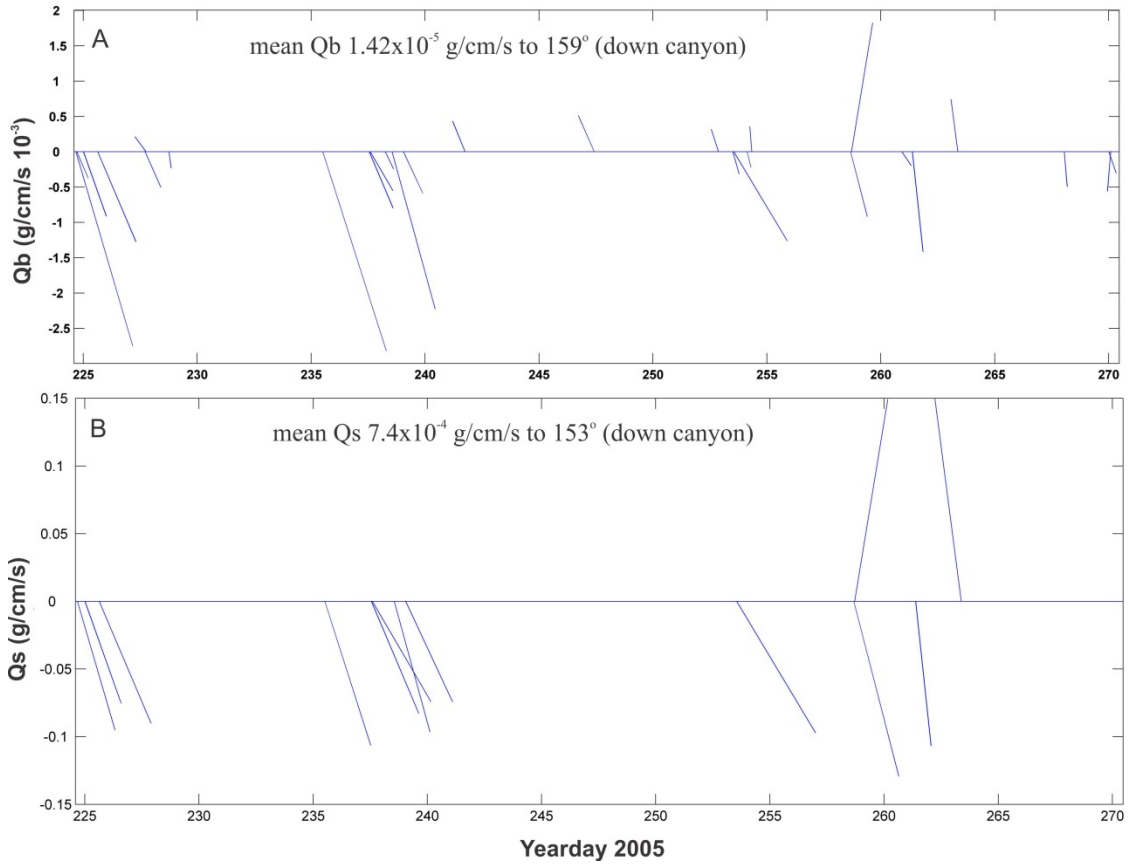

Figure 20 Vectors of the estimated (a) bedload and (b) suspended-load transport rates for the 2005 Logan Canyon deployment. Mean transport rates and directions are also shown. Top of the diagrams is the magnetic north. Note the different scales for the estimated bedload and suspended-load transport rates.

5. SUMMARY

The GSCA instrumented seabed lander RALPH was deployed in August 2005 in ~278 m depth in the head of Logan Canyon to provide the first field observations of near-bed hydrodynamics and sediment transport processes on the floor of a canyon on the Scotian Slope. The relatively long deployment recorded nearly 3 neap-spring tidal cycles and the maximum tidal range was ~2 m. Hourly-mean near-bed currents were up to 35 cm/s although peak instantaneous currents could reach as high as 40 cm/s. The peak bottom currents were predominantly in the along-canyon direction (NW–SE). Along-canyon currents were typically 2-3 times higher than the cross-canyon currents. The peaks of down-canyon currents were stronger

and more frequent than the up-canyon currents which led to a 4 cm/s mean current in the down-canyon direction.

Detailed comparisons of bottom mean currents and tidal elevation changes demonstrate that the bottom currents were highly variable with periods as short as 2 hours. Although the high variability is related to the forcing by the semi-diurnal tides, the bottom currents show much higher frequencies. Analyses of 30 minute instantaneous velocity data for individual and multiple bursts reveal that the observed high-frequency current peaks are asymmetric pulses of up- and down-canyon currents that resemble the “tidal bore” features. The tidal bores typically last 2 to 5 hours. However, the fronts of up-canyon bores build up quickly and the reversal to down-canyon flows occurs more gradually. The down-canyon bores also show higher speeds and last longer than the up-canyon bores. The correlation between the along-canyon tidal excursion and the rise and fall of the temperature confirms that the observed high-frequency strong bottom current pules were internal tide bores formed due to the focused tidal energy by the v-shaped geometry of the canyon.

Concurrently collected seabed imageries and suspended sediment concentration measurements show that the strong and highly variable bottom currents were strong enough to cause numerous bedload and suspended-load transport events. Suspended sediment concentrations in strong current events were generally 5 – 10 mg/l higher than the background means and the maximum concentrations near the bottom reached nearly 100 mg/l. The peaks of the suspended sediment concentration were generally correlated with that of the bottom currents. Furthermore the increase of sediment concentration above the background value was the highest close to the seabed and decreased with height away from the bottom. These would suggest that the sediment suspension associated with strong currents was bottom intensified due to erosion and resuspension of the local sediments.

Comparisons of bottom currents with the critical velocity for bedload and suspended-load transport suggest that the fine sand sediments in the head of Logan Canyon was transported in bedload in 2.1% of the time and in suspended-load in 1.2% of the time for the deployment duration. Based on the measured bottom currents and near-bed suspended sediment concentration, it was estimated that bedload transport peaks typically reached 0.003 g/cm/s while suspended-load transport reached the maximum value of 0.15 g/cm/s. Therefore suspended-load transport was dominant over bedload transport at the head of Logan Canyon. Down-canyon

transport was dominant for both bedload and suspended-load transport. The mean suspended-load flux averaged over the deployment was ~7.4 x 10^{-4} g/cm/s in the down-canyon direction.

Previous studies have suggested that sediments transported by storms on the shelf would spill into the heads of canyons on Scotian Slope (Hill and Bowen, 1983; Mosher et al., 2004). Canyon channels therefore may accumulate sand occasionally during the Holocene (Piper, 2001; Campbell and MacDonald, 2006). Two moderate storms with wind speeds > 16 m/s occurred during the lander deployment. Due to the deep water depth at the head of Logan Canyon, the storms did not affect the bottom currents. However, peaks of substantially high sediment concentration were recorded approximately 2 days after the storms. These peaks showed gradual build up, lasted more than 24 hours and were not bottom intensified, suggesting they were likely spilled over from sediments transported by storms on the shelf and then advected down canyon to the lander deployment site. The strong bottom current pules of internal tidal bores and the resulting episodic intensive sediment erosion and transport observed at the head of Logan Canyon could be a potential triggering mechanism for sediment mobilization and turbidity current formation in canyons on the Scotian Slope margin.

ACKNOWLEDGEMENTS

The authors would like to thank David Piper, Edward King, and Calvin Campbell for discussions of canyon-related seabed instability issues and the selection of the deployment site. We would like to thank Bob Murphy and the captain and crew of CCGS Sir William Alexander for their support for the deployment of RALPH. We appreciate the collaboration efforts of Don Gordon and John Anderson (DFO) and Gordon Fader during the DFO October 2005 Hudson expedition. We are especially grateful to Dick Pickrill for connecting us to DND, to Lt. Cdr. Jim Bradford of DND for coordinating the recovery operation, and to DND's DSIS ROV unit and the crew of CCGS Sir Wilfred Grenfell for their excellent work in the recovery of RALPH. David Piper reviewed this report and provided many useful comments. This project was jointly funded by Earth Science Sectors Geosciences for Ocean Management Program and the Program of Energy Research and Development (PERD) through the Pipeline POL (Program at Objective Level).

References

Bagnold, R.A., 1966. An approach to the sediment transport problem from general physics. US Geological Survey Professional Paper, 4421, 37pp.

Brown, C.B. 1950. Sediment transportation. In: Engineering Hydraulics, Edited by Rouse, H., New York, John Wiley and Sons, 796p.

Butman, B., 1988, North Atlantic Slope and Canyon Study, Volume 2: U.S. Geological Survey Open-File Report 88–27B: http://pubs.er.usgs.gov/djvu/OFR/1988/orf_88_27_b.djvu

Campbell, D.C. and MacDonald, A.W.A., 2006. Geohazard Assessment of Five Deepwater Pipeline Scenarios on the Scotian Slope, Geological Survey of Canada, Open File 5079, 48 p.

Dupont, F., Hannah, C.G. and Greenberg, D., 2005. Modelling the sea level in the upper Bay of Fundy. Atmosphere-Ocean 43, 33-47.

Dyer, K.R., 1986. Coastal and estuarine sediment dynamics. Wiley & Sons, Chichester, Engl., 342 pp.

Gardner, W.D., 1989. Periodic Resuspension in Baltimore Canyon by Focusing of Internal Waves. Journal of Geophysical Research, 94 (C12), 18185-18194.

Heffler, D.E., 1996. RALPH - A dynamic instrument for sediment dynamics. Proc. Oceans'96, IEEE, Ft. Lauderdale, Florida, USA, September 1996, p. 728-732.

Hill, P.R. and Bowen, A.J. 1983. Modern sediment dynamics at the shelf slope boundary off Nova Scotia; in The Shelfbreak. Critical Interface on Continental Margins, eds. D.J. Stanley and G.T. Moore; Society of Economic Palaeontologists and Mineralogists Special Publication No. 33, p. 265-276.

King, E.L. Fader, G.B.J., Lynds, T., Hynes, S. and Miller, R.O., 2002. Blue Atlantic Pipeline Corridor Geologic Constraints, Scotian Shelf: Desktop Study. Technical report to Accent Engineering Consultants Incorporated, from Geological Survey of Canada-Atlantic. 197pp.

Li, M.Z. and Heffler, D.E., 2002. Continental Shelf Sediment Transport Studies in Canada: Basic Theories and Recent Technology Advances. Environmental Marine Geoscience 3, Geoscience Canada, 29, 35-48.

Li, M.Z., Hannah, C.G., Perrie, W.A., Tang, C.C.L., Prescott, R.H. and Greenberg, D.A., 2015. Modelling Seabed Shear Stress, Sediment Mobility and Sediment Transport in the Bay of Fundy. Canadian Journal of Earth Sciences, 52, 757-775, 10.1139/cjes-2014-0211.

Miller, M.C., McCave, I.N. and Komar, P.D., 1977. Threshold of sediment motion under unidirectional currents. Sedimentology, 24, 507–527.

Mosher, D.C., Piper, D.J.W., Campbell, C. and Jenner, K.A., 2004. Near surface geology and sediment-failure geohazards of the central Scotian Slope. AAPG Bull., 88, 703–723.

Noble, M. A. and Xu, J. P., 2003. Observations of large-amplitude cross-shore internal bores near the shelf break, Santa Monica Bay, CA. Marine Environmental Research, 56, 127-149.

Piper, D.J.W., 2001. The geological framework of sediment instability on the Scotian Slope: studies to 1999. Geol. Surv. Can., Open File 3920, 202 pp.

Rosenfeld, L.K., Paduan, J.D., Petruncio, E.T. and Goncalves, J.E., 2002. Numerical Simulations and Observations of the Internal Tide in a Submarine Canyon. Ocean Modelling, 4, 1-8.

Swail, V. R., Cardone, V.J., Ferguson, M., Gummer, D. J., Harris, E. L., Orelup, E. A. and Cox, A. T., 2006. The MSC50 Wind and Wave Reanalysis, paper presented at 9th International Workshop on Wave Hindcasting and Forecasting, Sep. 25-29, 2006, Victoria, B.C. Canada.